16. CARBONATE DIAGENESIS AT SITE 308 KŌKO GUYOT

Albert Matter, Universität Bern, Bern, Switzerland
and
James V. Gardner, Scripps Institution of Oceanography, La Jolla, California

INTRODUCTION

Kōko Guyot is a large seamount located at the southern end of the Emperor Seamount chain (35°30'N, 171°45'E, Figure 1). Leg 32 of the Deep Sea Drilling Project crossed the southern portion of the guyot from the southwest, drilled Sites 308 and 309, and proceeded northeastward to complete the crossing.

A detailed study of the morphology and geology of Kōko Guyot is presented by Davies et al. (1972). The following description is a summary of their findings. The guyot rises to within 270 meters of the sea surface with a relatively flat upper surface bounded by steep slopes which descend to depths of 800 to 1200 meters. Two dredge hauls are reported by Davies et al. (1972), one from the western flank of the guyot which returned basalt and volcanic breccia (discussed by Clague and Dalrymple, 1973) and the other from the southern end of the plateau which collected reef limestones and cobbles of a variety of igneous rock types (Clague and Greenslate, 1972). Davies et al. (1972) calculated the thickness of the limestone cap to be 600 meters, comparable to that of the other Pacific atolls. Taking into account the present depth of the limestone cap, the optimum depth of reef growth of 30 meters, and the assumed 30 m.y. age of the seamount (taken from Jackson et al., 1972), Davies et al. (1972) concluded that reef growth terminated 5 to 6 m.y. ago. Leg 32 drilling results indicate that the age of Kōko Guyot is at least 50 to 51 m.y. old, early Eocene (*Discoaster lodoensis* Zone).

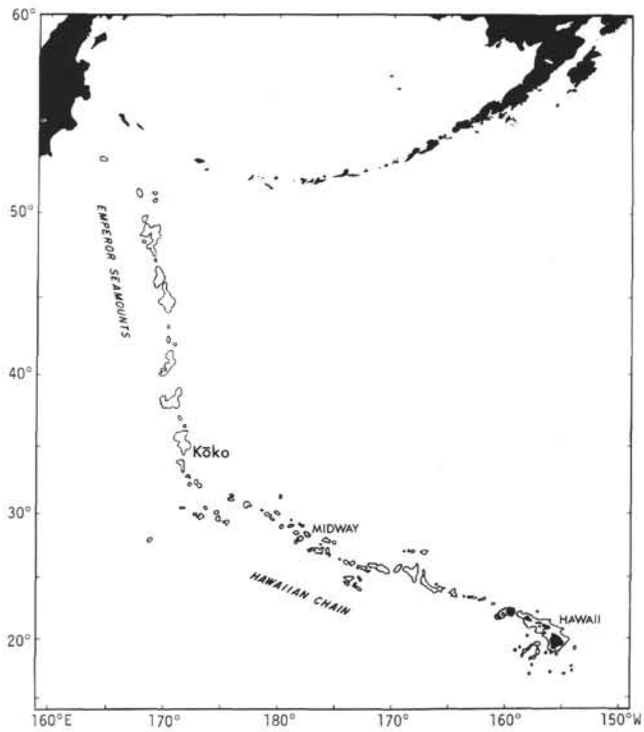

Figure 1. *Location of Kōko Guyot.*

SEDIMENTS

General Sediment Description

Site 308 is located on the southeastern edge of the plateau, downslope from the coral cap. Only four cores were recovered from Site 308 before drilling was terminated. The cores show a color change, from an oxidized dark yellowish-brown color at the top (Core 1) to oxygen-depleted dark gray color at the bottom (Cores 2, 3, and 4). The X-ray results suggest this change may be due to increasing pyrite contents with depth. The physical character of the cores correlates with the degree of cementation. Cores 1 and Section 1 of Core 2 are stiff uncemented sediment; Section 2 of Core 2, Core 3, and upper part of Core 4 semilithified; and the lower part of Core 4 is a well-cemented sandstone. An increase in grain size with depth is quite noticeable. A sharp contact occurs at 78 cm in Core 4 between the upper siltstone section and the lower sandstone (Figure 2). The upper silty sediments are altered volcanic ash composed of palagonite, glass shards, with rare bryozoa (Cheetham, this volume); ostracodes, benthonic foraminifera (Luterbacher, this volume); and some weathered carbonate fragments that resemble decomposed mollusk shells. The carbonate content is only 2% to 3%. Coarse sand-sized well-rounded volcanic rock fragments, benthonic foraminifera, bryozoa, ostracodes, coralline algae, and calcite cement all increase with depth until in Core 4 the sediment becomes a well-cemented biogenous volcanic sandstone. The only apparent internal structure is in the coarse grains which show a rough horizontal alignment and occasionally imbrication.

A biostratigraphic unconformity, based on nannofossils, occurs in Core 1 at approximately 70 cm depth separating Quaternary from lower Eocene sediments (see Biostratigraphic Summary, Site 308, this volume). However, this unconformity is not apparent from the lithology or color of the sediments.

Microfacies and Petrography

The early Eocene section drilled on Kōko Guyot shows three different microfacies (Figure 3):

1) A dark yellowish-brown, soft clayey silt was recovered in the top core. This silt consists mainly of

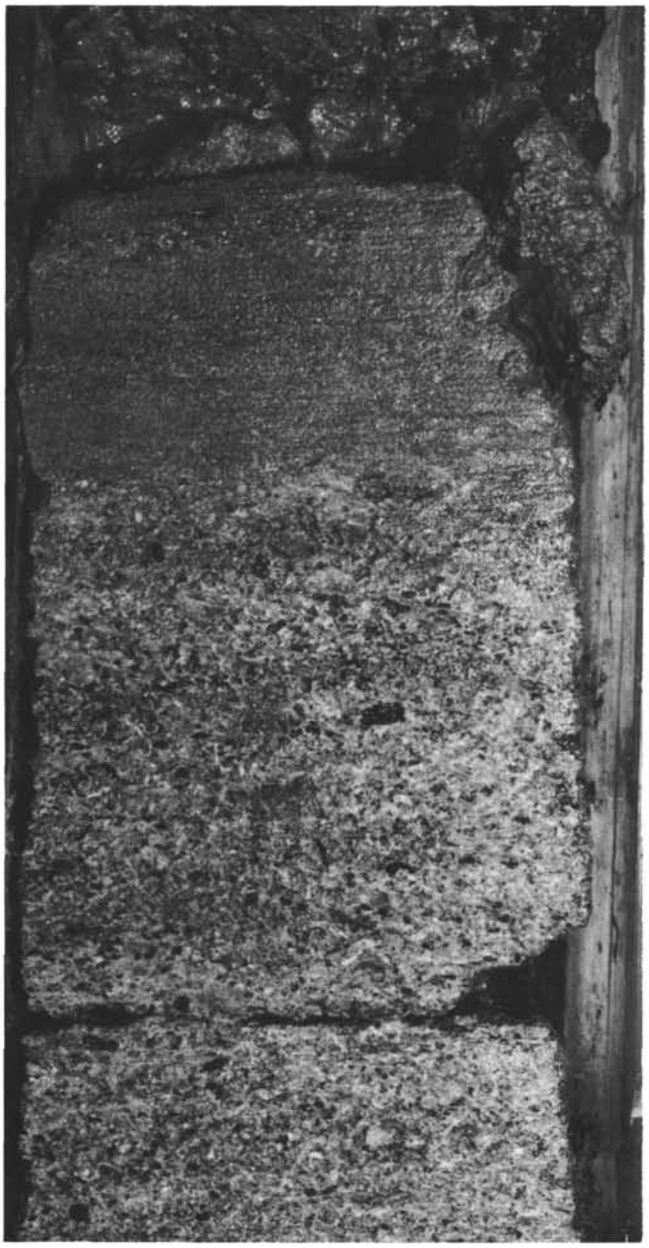

Figure 2. *Site 308, Core 4, Section 1, sharp lithologic break at 78 cm separating the lower sandstone from the upper siltstone.*

palagonite, light volcanic glass, montmorillonite, partly altered potassium feldspar and plagioclase, and lesser amounts of clinoptilolite, augite, and pyrite. Characteristically, this volcanic clayey silt is very low in carbonate (2% to 3%). Rare nannofossils, benthonic foraminifera, and bryozoa are seen in thin section and smear slides.

Clinoptilolite occurs as 2-25 micron long single and twinned crystals which are moderately corroded. The augite crystals (30-80 microns in size) are fresh but show cockscomb-like terminations indicating considerable intrastratal dissolution of this relatively unstable heavy mineral.

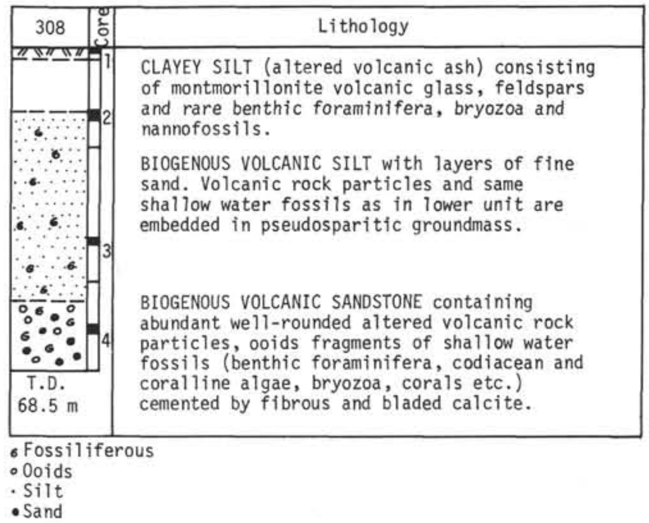

Figure 3. *Sequence of major lithologies drilled at Site 308, Kōko Guyot.*

This sediment probably represents an altered volcanic ash (see also lithologic description, Site 308 chapter).

2) A biogenous volcanic silt of medium dark gray color occurs in Cores 2 and 3 (Figure 3). Texturally, the sediment is mainly a clayey silt with occasional faint laminations, bioturbate structures, and rare interbedded layers of fine sand. The consolidation increases from stiff in Core 2 to semilithified in Core 3 due to progressive cementation and recrystallization of the carbonate particles and the calcareous groundmass. The carbonate content of bulk samples ranges from 43% to 63%.

This microfacies is characterized by abundant angular to rounded, sand- to silt-sized, highly altered volcanic rock and glass particles which are embedded together with skeletal fragments in a pseudosparitic groundmass (Figure 4). The major skeletal elements are, in order of decreasing abundance: benthonic foraminifera (perforate, porcelaneous, and arenaceous), bryozoa, and ostracodes. Planktonic foraminifera, echinoderm remains, and fragments of pelecypods and coralline algae are rare.

A few ovoid to slightly irregularly shaped ooids were observed ranging in size from 20 to 30 microns. They show a brown ferruginous stain and pyrite inclusions concentrated in the outermost part of the cortex. These ooids are micritic, have a faint concentric structure, and show pronounced thin radial fibers. The core of the ooids is either a volcanic rock fragment or a bioclast. The cortex measures between 0.5 and 0.6 of the ooid radius.

Pyrite and ilmenite are conspicuous as minor constituents (see Zemmels and Cook, this volume). Framboidal pyrite occurs mainly in chambers of foraminifera and other fossils. Where pyrite is found in the groundmass and in grains of volcanic rocks, it occurs dominantly as tiny single cubes and aggregates of cubes.

3) Biogenous volcanic sandstone. This microfacies is restricted to the lowest section sampled (Core 4) at Site 308 (Figure 3). It consists mainly of well-rounded, sand-sized volcanic rock particles and different types of skeletal fragments that are cemented by fibrous and

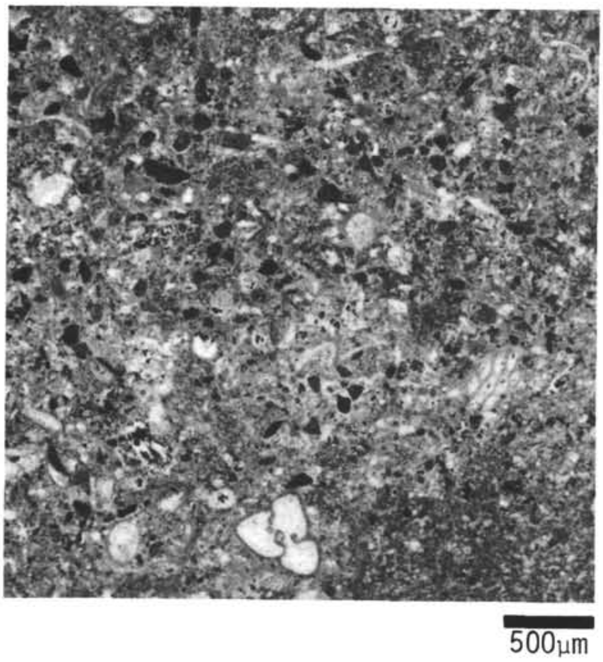

Figure 4. *Biogenous volcanic silt consisting of angular to rounded epiclastic volcanics, palagonite, and bioclasts embedded in a pseudosparitic groundmass. Thin section Sample 308-2, CC.*

sparry calcite (Figures 5 and 6). Although the abundance of the different constituents varies between thin sections taken at different levels, all the studied samples from Core 4 belong to a single characteristic microfacies.

The volcanic rock particles are flat, oval-shaped and occasionally imbricated (Figure 5). Commonly they have a superficial oolitic coating, 10 to 40 microns thick, or a thin (10 microns) crust of authigenic montmorillonite (Plate 3, Figures 3 and 6). The oolitic coating is generally absent on the rounded corners of the grains, indicating abrasion of the coating during movement of the grains.

The most abundant skeletal particles are benthonic foraminifera (perforate, porcelaneous, and arenaceous), bryozoa, and plates of *Halimeda,* a calcareous green alga. Ostracodes, lamellibranchs, gastropods, echinoderms, solitary corals, serpulidae, coralline algae, and some dasycladacean algae all occur but vary from common to rare in abundance. Both disarticulated branches and nodules (up to 1 cm in size) of coralline algae were observed. The serpulids were attached to hard substrates such as pelecypod shells, plates of calcareous green algae and bryozoan colonies (Figure 6). Miliolids are the most common porcelaneous foraminifera.

Ooid abundance ranges from 10% to 20% in some samples. Ooids occur as large single grains 0.15 to 0.25

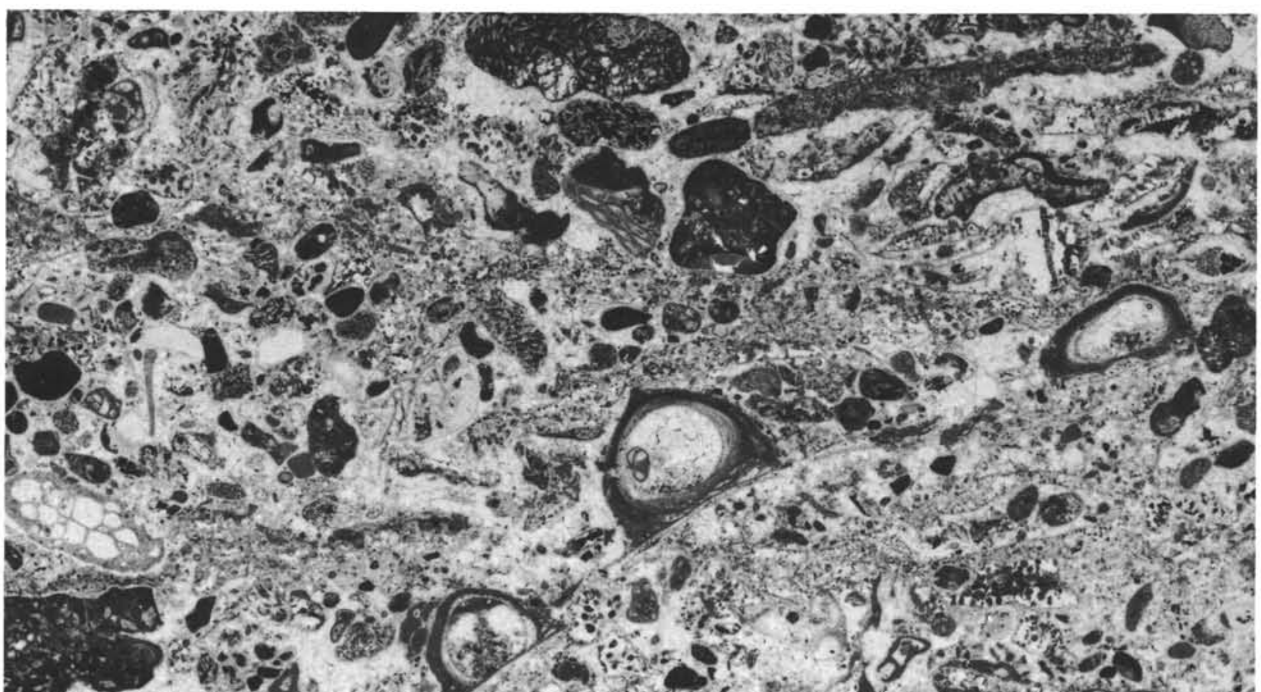

Figure 5. *Biogenous volcanic sandstone as in Figure 6, but with dominant epiclastic volcanics, common ooids, grapestones, and other intraclasts and few bioclasts. Many of the volcanic particles have a superficial oolitic coating. Notice their excellent roundness, flat shape and imbrication. Thin section Sample 308-4-1, 126 cm.*

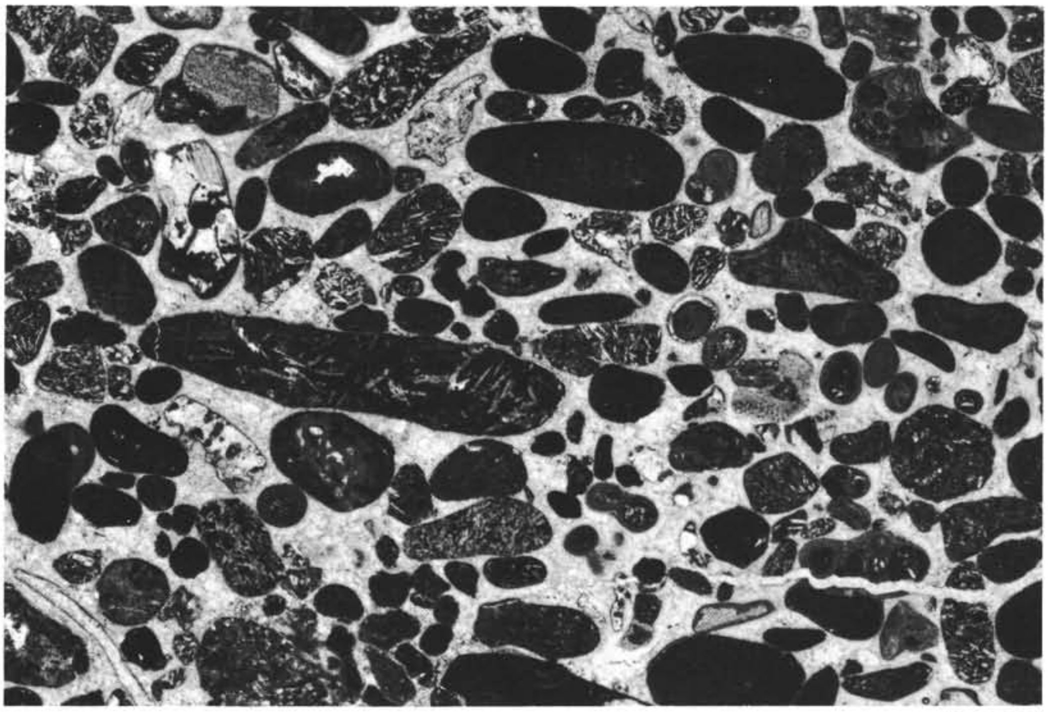

Figure 6. *Well-washed and moderately sorted biogenous volcanic sandstone consisting mainly of well-rounded epiclastic volcanics and bioclasts cemented by low-Mg sparry calcite.* Halimeda *plates, benthonic foraminifera, and bryozoa are the dominant skeletal remains. Notice serpulids growing on and encrusting bioclasts. Thin section Sample 308-4-1, 68 cm.*

mm in diameter as well as in grapestone lumps where they are associated with volcanic rock fragments and bioclasts. Intraclasts other than grapestones are also present in small amounts. The nuclei of the ooids are either altered volcanic rock particles or bioclasts, most frequently coralline algal fragments and tests of foraminifera. The radius of the ooid cortex generally equals that of the nucleus (Figure 5).

Ooids seen in thin section display alternate clear and yellow-brownish micritic layers. The clear layers consist of radially oriented neomorphous calcite crystals, whereas the darker layers are made up of minute grains ("nano-grains" of Loreau and Purser, 1973) when studied in the electron microscope (Plate 1, Figure 4). An identical relationship between micro- and ultrastructure of ooids has been described by Loreau and Purser (1973).

Pyrite is present in clusters of framboids in chambers of fossils, but it also occurs as tiny crystals in micritized tests.

The sediments within this microfacies are well sorted and only rarely contain patches of micritic groundmass. However, interbedded with microfacies 3, some layers of microfacies 2 were observed.

The carbonate content of the bulk sediment varies from 60% to 70%. This rock type, as well as the previous one, would be classified as a limestone on a chemical basis. However, taking into account the cement which contributes about 10% to 30% of the carbonate, the sediments described above are best classified as biogenous volcanic sandstone and biogenous volcanic silt.

Carbonate Mineralogy

The mineralogical composition of the calcareous skeletons, matrix, and cement was investigated with the aid of X-ray diffraction and electron microprobe analysis, combined with conventional thin-section examination.

Because of the different primary mineralogy of the rock-forming skeletal-carbonate constituents, the sediments at Site 308 originally consisted of a mixture of strontium aragonite, (corals, *Halimeda*, ooids); high magnesian calcite (coralline algae, miliolids); and low magnesian calcite (planktonic foraminifera, nannofossils).

However, all the grains which originally consisted of either of the metastable phases (aragonite and magnesian calcite) have been converted to stable low magnesian calcite with less than 4 mole % $MgCO_3$ (bulk analysis).

Thin sections were stained for aragonite and high-Mg calcite but no relicts of these minerals were discovered. Strontium, although not measurable quantitatively, was observed in the micritic parts of ooids, suggesting the presence of relicts of aragonite microcrystals.

DIAGENESIS

The flood of scientific articles on shallow-water carbonates published during the past 20 years has greatly increased our understanding of how accumulations of metastable aragonitic and Mg-calcitic particles become stabilized and lithified. Stabilization and lithification take place most rapidly when the sediments are exposed to the vadose and meteoric realm. However, during the last few years increasing evidence for submarine diagenesis and cementation has been cited (Bathurst, 1971; Milliman, 1974).

Because the alteration of carbonate grains in shallow-water sediments has been widely studied, we will only briefly describe the diagenetic features of some Mg-calcitic and aragonitic grains. Then we will describe in greater detail the ultrastructure and fabrics of the carbonate cement and discuss their origin.

Alteration of Carbonate Grains

The alteration of carbonate grains at Site 308 is best studied in the coarse-grained biogenous volcanic sandstone which contains abundant grains composed originally of metastable aragonite or Mg-calcite. The behavior of grains during diagenesis, and thus the ultimate state of preservation of different kinds of skeletal and nonskeletal carbonate grains, depends largely on their initial mineralogy.

The most abundant strontium-rich aragonitic particles are plates of the calcareous green alga *Halimeda* and ooids (Figures 5 and 6). The flakes of living *Halimeda* consist of intertwined and branching filaments or utricles which are more or less calcified by fused aragonite needles (Milliman, 1974). Infilling of the utricles by secondary aragonite needles (Glover and Pray, 1971; Marszalek, 1971) or high-Mg calcite or with both minerals (Winland, 1971) starts soon after burial, rendering greater strength to the algal plates. Milliman (1974) also reports disc-like secondary aragonite in the utricles.

In our Eocene material from Site 308, the calcified filaments have been dissolved to various degrees and in a patchy manner. The aragonite of the remaining filaments, their secondary carbonate infillings, as well as the micrite envelope, were subsequently replaced by microcrystalline low-Mg calcite. The intraparticle void space (primary and secondary) is partly filled with fibrous and bladed calcite cement (Plate 1, Figure 1). Progressive replacement of micrite by calcite spar results in a finely crystalline blocky calcite fabric leaving no trace of the primary skeletal structure in thin section. As shown by Schneidermann et al. (1972) the micritic wall and the void-filling spar may become replaced by neomorphic spar (Plate 1, Figure 2) which may contain relict aragonite needles. In the advanced state of replacement, the algal origin of the particle is recognized only by the micrite envelope (Plate 1, Figure 2). Finally, the micrite envelope also may be replaced by coarser calcite crystals, resulting in a continuous mosaic of intraparticle and interparticle calcite cement. These results are similar to the observations made by Tebbutt (1967) on *Halimeda* plates of Pleistocene age.

Ooids which initially consisted of strontium-rich aragonite (see Carbonate Mineralogy section above) display yet another pattern of replacement by low-Mg calcite. As mentioned previously, the ooids cortices consist of alternating clear lamellae of radially oriented calcite and yellowish-brown micritic laminae made up of minute grains (Plate 1, Figure 3 and 4). Similar ooids were described by Hesse (1973) from the Ita Matai Seamount. The width of the clear lamellae and thus the size of the subequant calcite crystals range between 1 to 10 microns. Thin streaks of microcrystalline grains often separate individual clear cyrstals within a clear lamina (Plate 1, Figures 3 and 4).

Some ooids consist mainly of thicker clear calcite layers alternating with thin micritic layers, whereas others, such as the ooid shown on Plate 1, Figure 5, have mainly a thick yellowish-brown micritic cortex with only few clear layers. The micritic layers are composed of low-Mg calcite and possibly some relict aragonite grains and a cryptocrystalline clay mineral (possibly of the montmorillonite series) as well as diffuse iron-oxide (limonite?). The presence of the yellow clay mineral and the brown-red iron oxide renders a yellow-brown color to the micritic laminae.

The yellow-brown laminated zone of micrite seen in the ooid cortex shown in Plate 1, Figure 5 is much lower in calcium than the clear layers (Plate 1, Figure 6). Also, the micritic parts contain high concentrations of Si, Al, Mg, and Fe, all of which are present in much lower concentrations or missing in the clear laminae. Optical investigation of stained thin sections suggests that Si, Al, and also most of the Mg are located in clay minerals and Fe in limonite(?). The chemical composition of the calcite in the clear laminae is identical with that of the intergranular cement.

It appears that the layers of micrite correspond with the organic-rich layers of nano grains described in recent ooids by Loreau and Purser (1973). According to these authors, the layers of nano-grains alternate with clear layers of either radially or tangentially oriented elongated aragonite crystals.

Although ooid diagenesis has attracted much scientific effort since Eardley's (1938) classical paper (see Bathurst, 1971 for review; Hesse, 1973; Kahle, 1974; Sandberg, in press), a brief account on the diagenetic features of ooids encountered at Site 308 is justified because of their unusual content of clay minerals.

We observed in a few ooids primary clear layers which were partly dissolved and had a lining of first-generation micron-sized calcite (?) crystals. This suggests that layers of primary clear aragonite (Loreau and Purser, 1973) were dissolved and infilled by radially oriented low-Mg calcite crystals on a piecemeal basis, thereby avoiding collapse of the cavity. This mechanism was first envisaged by Shearman et al. (1970). These features have been documented with excellent SEM photomicrographs by Fabricius and Klingele (1970).

The clay minerals associated with minute carbonate grains not only occur in the concentric laminae of micrite, but also in the irregular, 1 to 5 micron wide "pillars" which separate the crystals of secondary calcite constituting the clear layers mentioned above (Plate 1, Figures 3 and 4).

The mode and time of formation of the clay minerals are not certain. They might either be of accretional or diagenetic origin. In the first case they would have been trapped during periods of ooid stability by the mucilaginous matter which coated the ooid surface. The diagenetic hypothesis assumes that the clays formed in primary or secondary pores generated by decay of organic matter and by dissolution of minute aragonite nano-grains. It appears that the "pillars" originated by growth of authigenic clay minerals in algal borings. By analogy, a diagenetic origin also is favored for the clay minerals in lamellae of the micritic ooids. Furthermore, authigenic montmorillonite predating deposition of calcite cement commonly coats volcanic grains in the studied samples. Therefore, the microenvironment was apparently very favorable to the formation of this clay mineral at times of very early diagenesis. The textural relationships indicate that the clay minerals and microcrystalline carbonate grains predate growth of secondary calcite in the clear laminae.

The diagenetic alteration, and thus the preservation, is different for the most common Mg-calcite particles, namely coralline algae and miliolid foraminifera. In all of the specimens studied the magnesium is gone (less than 4 mole % $MgCO_3$).

The skeletal microstructure of altered coralline algae is almost always well preserved in ancient sediments. Land (1967) suggested that magnesium is selectively removed and replaced by calcium through incongruent dissolution. Although this process is not understood in detail, it apparently does not involve a void stage, and thus would explain the perfect preservation of coralline algae.

Unlike coralline algae, miliolid foraminifera, which have an amber color and are translucent and cryptocrystalline under the microscope, are frequently replaced by microcrystalline low-Mg calcite. Usually miliolid tests first become spotted with micrite grains which increase in number until finally the entire test is micritized (Plate 2, Figures 1 and 2). High-Mg calcite echinoderm fragments altered to low-Mg calcite show the same sequence of replacement features (see, also, Crickmay, 1945).

Our data are insufficient to determine whether this alteration takes place by dissolution-reprecipitation beneath a mucilaginous envelope (Kendall and Skipwith, 1969) or by boring and subsequent precipitation of tiny carbonate crystals in the excavated tunnels as described by Bathurst (1966) and Alexandersson (1972). Neither of these mechanisms provides a sufficient explanation for the different state of preservation of the coralline algae and miliolids.

Moreover, it is not entirely clear why the mineralogic transformation from aragonite to calcite generally is texturally destructive. However, it does involve a dissolution-reprecipitation mechanism with an intermediate void stage as mentioned above. Purdy (1968) questioned the validity of "incongruent dissolution" as a mechanism for mimicry of biogenic fabrics and pointed out that perhaps the problem of textural preservation or destruction is only a matter of the scale of the same dissolution-reprecipitation process. Dissolution and reprecipitation on the ultramicroscopic scale would appear texturally nondestructive in the light microscope. The textures would be destroyed only where larger cavities are formed.

However, the most recent results on neomorphic replacement of aragonitic skeletons by calcite (Schneidermann et al., 1972; Sandberg, in press) do not support Purdy's hypothesis. Although the neomorphic process appears to operate along thin-film fronts without formation of visible voids, it is texturally destructive and results in a coarse neomorphic calcite fabric which may or may not contain relic structures.

Habit and Fabrics of Calcite Cements

The ultrastructure and the fabrics of carbonate cements are best developed in the biogenous volcanic sandstone because of its high initial porosity (at least 40%) and the large size of the pores. Cement lines or fills interparticle and intraparticle voids. Two kinds of cements are found: palisade cement consisting of fibrous crystals and blocky cement made up of blade-like crystals. No needle-like cement occurs in these sediments. Where both cements occur together, palisade cement always forms the first crust on the grains. Where the crystals rise from a polycrystalline substrate, which provides a high nucleation rate (such as oolitic coatings, porcelaneous foraminifera, coralline algae, or micrite envelopes), they are subparallel, radiate very regularly, and increase in length towards the center of the pore (Plate 2, Figure 5 and Plate 3, Figure 4). The correlation between regularity of crystal orientation and crystal density was pointed out by Schroeder (1972).

The length of the crystals is highly variable and ranges from less than 10 microns up to 150 microns. Very small (<10 microns) fibrous crystals, which are rooted on the sediment grains and which themselves serve as a substrate for larger fibrous crystals, are faintly recognizable in thin sections. It is possible that the latter are composite crystals of several tiny fibrous crystals which have been overgrown by larger ones. In linings with high crystal density, the fibrous crystals have an almost constant width which decreases only slightly towards the tip (Plate 2, Figure 6). The ratio of length to width varies between 3 and 10. Commonly, the crystals terminate with two sets of rhombic faces which are rotated 60° against each other (Plate 3, Figure 1 and Schroeder, 1972, fig. 5d). Steep rhombic faces form the long sides of the crystals. The terminal part of the long sides of the crystals often shows curved faces (Plate 3, Figure 1).

Substrates on which cement would have a slow nucleation rate, such as volcanic grains coated with a thin layer of authigenic clay (Plate 3, Figure 3), are lined with subequant crystals about 5 microns in length. These abut against bladed to blocky calcite spar. If the subequant crystals are missing, bladed or blocky calcite is in direct contact with the detrital grains (Plate 3, Figure 3).

The true nature of the bladed crystals, which grew rooted on fibrous or subequant crystals, is best seen in samples only partially cemented. As shown in Plate 3, Figures 2 and 4, the bladed crystals are steep-sided composite crystals which consist, at their base, of several smaller crystals. The composite crystals reach about 350 microns in length and decrease stepwise in width towards the tip, where they almost always terminate with crystal faces and never show the depressions characteristic of the submarine aragonite cement described by Schroeder (1972). Because the bladed crystals nucleate rather irregularly and are wider spaced than the fibrous crystals, the growth direction of the bladed forms is less controlled and therefore often oblique to the substrate.

If the crystal blades arrive from different directions, they interfere with each other in an intergranular pore and display a bulky fabric (Plate 3, Figures 4 and 5). As they continued to grow, they fill the pore completely (Plate 3, Figure 6). Such pore fillings show, in thin section, all the characteristics of blocky calcite spar (Bathurst, 1971, p. 417). In this case the sparry calcite mosaic is caused by growth of blade-like calcite crystals, whereas in deep-sea chalk the same fabric results from growth of equant calcite rhombohedrons (Matter, 1974, Pl. 9, fig. 6).

Microprobe profiles run across fibrous crusts and into blocky calcite cement revealed that the concentrations of $MgCO_3$ decreased from about 3 mole % $MgCO_3$ close to the substrate to 1.6 mole % $MgCO_3$ in the blocky calcite. Traces of iron were also observed, but no strontium was detected.

Syntaxial overgrowths on crinoid fragments are common in Core 4 (Evamy and Shearman, 1965; 1969). In the same sample some crinoid fragments may have a syntaxial overgrowth, and others may have a crust of fibrous calcite cement whose crystals are not in lattice continuity with the host. Apparently, growth of the latter calcite crystals is favored on crinoid fragments which have an oolitic coating or a micrite rim.

In the porous biogenous volcanic sandstone two basically different kinds of cement fabrics were observed. The cement shown in Plate 2, Figure 5 is characterized by subparallel fibrous calcite forming thick coatings on the grains and relatively few bladed composite crystals. The bladed crystals occupy, as second generation cement, the interior of some pores. A sutured contact is seen in thin sections (Plate 2, Figure 3) where fibrous crusts meet and fill entire pores. The same kind of cement fabric has been described by Cullis (1904) from Funafuti (see Bathurst, 1971, fig. 269). Of course, changes in the relative amounts of fibrous to bladed crystals vary the aspect of this basic fabric (Plate 2, Figure 4). Such changes are present within the range of a single sample.

The second type of cement fabric observed in Core 4 is shown on Plate 2, Figures 1 and 2. A thin layer of first-generation subequant-micritic crystals is followed by last-generation bladed-composite crystals which occlude most of the intergranular pore space. The bladed crystals form a sparry mosaic which shows some of the criteria, such as straight boundaries and enfacial junctions, which, are diagnostic for void-filling spar Bathurst (1971). It does not show, however, the increase of crystal size towards the center of the pore.

CONCLUSIONS

The abundance of shallow-water benthonic foraminifera, calcareous green algae, coralline algae, and ooids in Core 4 indicates that the biogenous volcanic sandstone accumulated in a water depth of less than 4 to 6 meters. Furthermore, the coarse-grained, well-rounded and moderately sorted nature of the sediment and the absence of a micritic matrix suggest mechanical abrasion and winnowing in a high-energy environment, such as the surf zone or lower foreshore. The sharp contact between the sandstone and the siltstone represents the change from a high-energy environment to a low-energy environment, possibly as the surface subsided below wavebase.

Many of the carbonate grains in the studied sediments have been micritized to various degrees by boring algae and fungi while still at or close to the sea floor. Many borings have been infilled by early diagenetic montmorillonite instead by micrite. This clay mineral also forms thin fringes around volcanic grains. Neoformation of montmorillonite thus predates deposition of the carbonate cements.

The Eocene sediments from Kōko Guyot have reached the diagenetic stage V of Land et al. (1967), i.e., Mg-calcite has lost its magnesium, most of the aragonitic particles have been dissolved, and much of the primary and secondary pore space has been cemented by what is now low-Mg calcite.

Generally bladed calcite, frequently forming a blocky fabric, succeeds either fibrous calcite fringes or thin crusts of subequant micritic crystals. Two main questions arise as to their origin: (a) are the crystals in their original mineralogical and chemical state? and (b) in which diagenetic environment did they grow?

Aragonite cement in shallow-water sediments commonly occurs as fibrous or needle-like crystals. The fibrous habit is not indicative for aragonite only because fibrous high-Mg calcite rim cement also has been described (Taylor and Illing, 1969; Schroeder, 1973; and others). However, from the absence of orthorhombic symmetry and absence of even traces of strontium, aragonite can be precluded as a precursor of the fibrous low-Mg calcite cement found at Site 308 (A. Stalder, personal communication).

Lindholm (1972) suggests that the amount of magnesium present in what is now low-Mg calcite might give a clue to its original mineralogy (low- vs high-Mg calcite). The relatively high magnesium content (approx. 3 mole % $MgCO_3$) together with the regular outline and fabric of the fibrous crystals may indicate that they are an ancient analog of the submarine high-Mg calcite palisade cement described by Schroeder (1972; 1973). Because the $MgCO_3$ content is only slightly lower in the bladed cement (approx. 1.5 mole %) and because no hiatus is observed between the two cement generations, the bladed composite crystals might have been deposited as high-Mg calcite as well. However, lacking any safe criterion or set of criteria which would allow a determination of the kind of primary calcite in our Eocene samples, the possibility that it has grown as low-Mg calcite cannot be ruled out with certainty.

In the absence of any features diagnostic of the vadose environment, it is concluded that the carbonate cements are of submarine origin.

ACKNOWLEDGMENTS

G. Burri, A. Mahé (Lausanne), and H. Walter generously carried out analyses with the microprobe and H. Ischi helped with the evaluation of the data. F. Zweili kindly operated the SEM and gave valuable technical advice. U. Ernst and U. Furrer prepared the photomicrographs, and Miss S. Sahli typed the manuscript.

F. Allemann and R. Herb helped with the identification of fossils, and A. Stalder gave advice on crystal morphology. R.N. Ginsburg and J.D. Milliman reviewed the manuscript. We thank all these individuals for their help and constructive criticism.

REFERENCES

Alexandersson, T., 1972. Micritization of carbonate particles: Processes of precipitation and dissolution in modern shallow-marine sediments: Geol. Inst. University of Uppsala Bull., new ser., v. 3, p. 201-236.

Bathurst, R.G.C., 1964. The replacement of aragonite by calcite in the molluscan shell wall. *In* Imbrie, J. and Newell, N.D. (Eds.), Approaches to paleoecology: New York (Wiley), p. 357-376.

———, 1966. Boring algae, micrite envelopes and lithification of molluscan biosparites: Geol. J., v. 5, p. 15-32.

———, 1971. Carbonate sediments and their diagenesis: Amsterdam (Elsevier).

Clague, D.A. and Greenslate, J., 1972. Alkali volcanic suite from the Emperor Seamounts: Geol. Soc. Am., Abstracts, v. 4, p. 136.

Clague, D.A. and Dalrymple, G.B., 1973. Age of Kōko Seamount, Emperor Seamount chain: Earth Planet. Sci. Lett., v. 17, p. 411-415.

Crickmay, G.W., 1945. Petrography of limestones. *In* Ladd, H.S. and Hoffmeister, J.E. (Eds.). Geology of Lau, Fiji: Bernice P. Bishop Mus. Bull., v. 181, p. 211-250.

Cullis, C.G., 1904. The mineralogical changes observed in the cores of the Funafuti borings. *In* Bonney, T.G. (Ed.), The Atoll of Funafuti: Roy. Soc. London, p. 392-420.

Davies, T.A., Wilde, P., and Clague, D.A., 1972. Kōko Seamount: a major guyot at the southern end of the Emperor Seamounts: Marine Geol., v. 13, p. 311-321.

Eardley, A.J., 1938. Sediment of Great Salt Lake, Utah: Am. Assoc. Petrol. Geol. Bull., v. 22, p. 1305-1411.

Evamy, B.D. and Shearman, D.J., 1965. The development of overgrowths from echinoderm fragments: Sedimentology, v. 5, p. 211-233.

———, 1969. Early stages in development of overgrowths on echinoderm fragments in limestones: Sedimentology, v. 12, p. 317-322.

Fabricius, F. and Klingele, H., 1970. Ultrastrukturen von Ooiden und Oolithen: Zur Genese und Diagenese quartärer Flachwasserkarbonate des Mittelmeeres. Verh. Geol. Bundesanstalt Wien, Jg. 1970, v. 4, p. 594-617.

Glover, E.D. and Pray, L.C., 1971. High-magnesium calcite and aragonite cementation within modern subtidal carbonate sediment grains. *In* Bricker, O.P. (Ed.), Carbonate cements: Baltimore and London (The Johns Hopkins Press), p. 80-87.

Hesse, R., 1973. Diagenesis of a seamount oolite from the West Pacific, Leg 20, DSDP. *In* Heezen, B.C., MacGregor, I.D., et al., Initial Reports of the Deep Sea Drilling Project, Volume 20: Washington (U.S. Government Printing Office), p. 363-387.

Jackson, E.D., Silver, E.A., and Dalrymple, G.B., 1972. Hawaiian-Emperor chain and its relation to Cenozoic circumpacific tectonics: Geol. Soc. Am. Bull., v. 83, p. 601-618.

Kahle, C.F., 1974. Ooids from Great Salt Lake, Utah, as an analogue for the genesis and diagenesis of ooids in marine limestones: J. Sediment. Petrol., v. 44, p. 30-39.

Kendall, C.G. ST.C. and Skipwith, P.A.D'E, 1969. Holocene shallow-water carbonate and evaporite sediments of Khor al Bazam, Abu Dhabi, southwest Persian Gulf: Am. Assoc. Petrol. Geol. Bull., v. 53, p. 841-869.

Land, L.S., 1967. Diagenesis of skeletal carbonates: J. Sediment. Petrol., v. 37, p. 914-930.

Land, L.S., Mackenzie, F.T., and Gould, S.J., 1967. Pleistocene history of Bermuda: Geol. Soc. Am. Bull., v. 78, p. 993-1006.

Lindholm, R.C., 1972. Magnesium content and crystal habits in ancient carbonates: Nature, Phys. Sci., v. 237, p. 43-44.

Loreau, J.-P. and Purser, B.H., 1973. Distribution and ultrastructure of Holocene ooids in the Persian Gulf. *In* Purser, B.H. (Ed.), The Persian Gulf. Holocene carbonate sedimentation and diagenesis in a shallow epicontinental sea: Berlin and New York (Springer), p. 279-328.

Marszalek, D.S., 1971. Skeletal ultrastructure of sediment producing green algae. *In* Johari, O. and Corvin, I. (Ed.), Scanning electron microscopy 1971: Ann. Scanning Electron Microscope Symp., 4th Proc., p. 275-280.

Matter, A., 1974. Burial diagenesis of pelitic and carbonate deep-sea sediments from the Arabian Sea. *In* Whitmarsh, R.B., Weser, O.E., Ross, D.A., et al., Initial Reports of the Deep Sea Drilling Project, Volume 23: Washington (U.S. Government Printing Office), p. 421-469.

Milliman, J.D., 1974. Marine carbonates. *In* Milliman, J.D., Müller, G., and Förstner, U. (Eds.), Recent Sedimentary carbonates, Part 1: Berlin and New York (Springer).

Purdy, E.G., 1968. Carbonate diagenesis: an environmental survey: Geol. Romana, v. 7, p. 183-228.

Sandberg, P.A., in press. New interpretations of Great Salt Lake ooids and of ancient nonskeletal carbonate mineralogy: Sedimentology.

Schneidermann, N., Sandberg, P.A., and Wunder, S., 1972. Recognition of early cementation of aragonitic skeletal carbonates. Nature, Phys. Sci., v. 240, p. 88-89.

Schroeder, J.H., 1972. Fabrics and sequences of submarine carbonate cements in Holocene Bermuda cup reefs. Geol. Rundschau, v. 61, p. 708-730.

———, 1973. Submarine and vadose cements in Pleistocene Bermuda reef rock: Sediment. Geol., v. 10, p. 179-204.

Shearman, D.J., Twyman, J., and Karimi, M.Z., 1970. The genesis and diagenesis of oolites. Proc. Geol. Assoc. (Engl.), v. 81, p. 561-575.

Taylor, J.M.C. and Illing, L.V., 1969. Holocene intertidal calcium carbonate cementation, Qatar, Persian Gulf: Sedimentology, v. 12, p. 69-107.

Tebbutt, G.E., 1967. Diagenesis of Pleistocene limestone on Ambergris Cay, British Honduras: Ph.D. thesis, Rice University, Houston, Texas, 133 pp. (unpublished).

Winland, H.D., 1971. Nonskeletal deposition of high-Mg calcite in the marine environment and its role in the retention of textures. *In* Bricker, O.P. (Ed.), Carbonate cements: Baltimore and London (The Johns Hopkins Press), p. 278-284.

PLATE 1
Diagenesis of aragonitic particles

Figure 1	Photomicrograph of *Halimeda* which now consists of low-Mg calcite. Utricles which had been infilled by ?high-Mg calcite (Winland 1971) and micrite envelope are preserved whereas the aragonitic thallus has been dissolved. The secondary intraparticle void space is being infilled by small fibrous acicular calcite crystals which are rooted on the utricles. Note similar habit of intra- and interparticle calcite cement. Thin section. Sample 308-4-1, 126 cm.
Figure 2	*Halimeda* plate replaced by neomorphic calcite. In the microscope brownish-stained neomorphic spar is seen where filaments have been replaced whereas clear spar marks former intrabiotic voids. Shape of *Halimeda* is retained by micrite envelope which also shows relicts of borings. Thin section. Sample 308-4-1, 58 cm.
Figures 3, 4	Scanning electron photomicrograph of strongly etched ooid showing alternation of clear calcite laminae (deeper etching) and micritic laminae. Under higher magnification (Figure 4) the micritic laminae as well as the micritic "pillars" separating clear calcite crystals are seen to consist of nanograins which are mainly montmorillonite and low-Mg calcite. Clear calcite has been etched away completely in Figure 4. Sample 308-4, CC.
Figure 5	Electron micrograph of ooid. Light laminae are micritic, darker ones are clear calcite. Inner part of cortical complex consists mainly of micritic layers. Note thick layer of clear calcite beneath outermost micritic lamina. Black line indicates where microprobe measurements have been made. Sample 308-4-1, 126 cm.
Figure 6	Beam scan image showing distribution of calcium in ooid of Figure 5. Nucleus which is a volcanic rock particle appears black. Micrite layers are recognized by their low concentration and clear calcite by high concentration. Sample 308-4-1, 126 cm.

PLATE 1

1 100µm

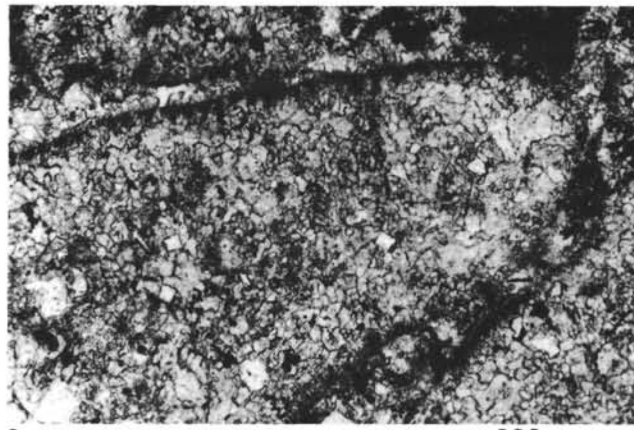

2 100µm

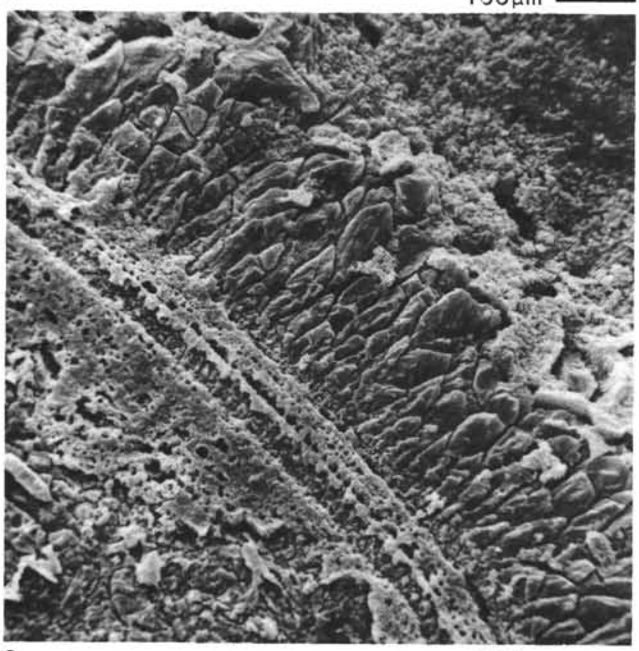

3 100µm

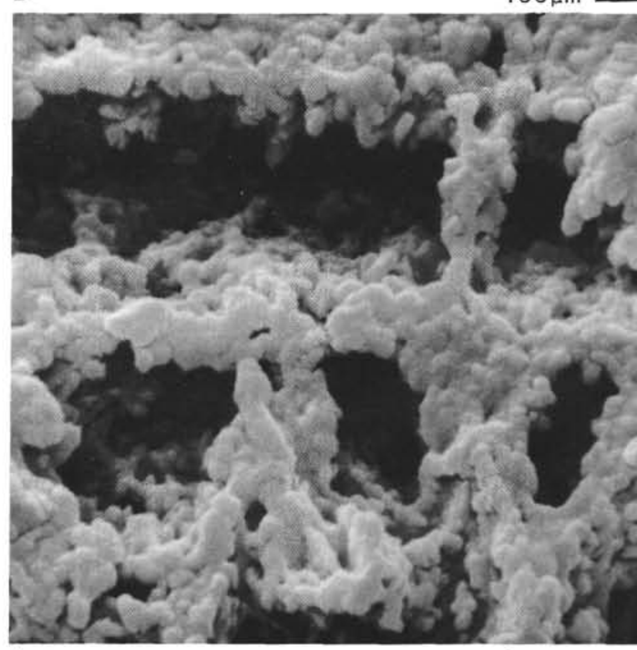

4 1µm

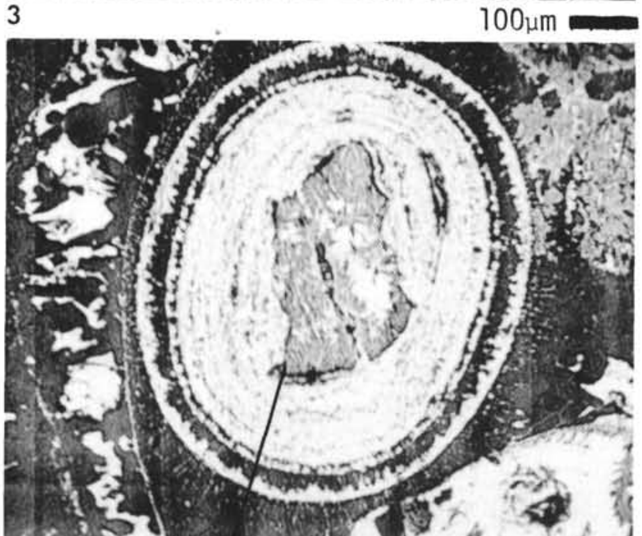

5 40µm

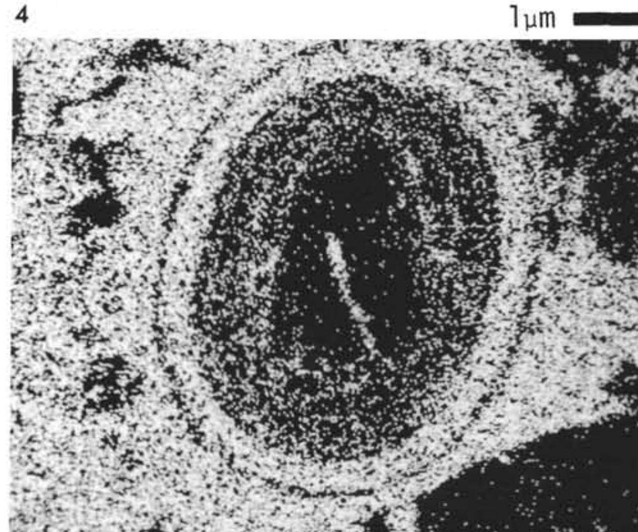

6 40µm

PLATE 2

Figures 1, 2	Cryptocrystalline miliolids, partly micritized in Figure 1 and completely micritized in Figure 2. Test shown in Figure 2 displays bores and a partly collapsed micrite wall. Collapse predates deposition of first-generation stubby calcite crystals which also grow on fracture surfaces. Notice coarse sparry calcite cement which immediately follows a thin layer of stubby first-generation crystals. Thin sections. Sample 308-4-1, 68 cm.
Figure 3	Fibrous palisade cement filling entire intergranular pore space. A sutured contact is seen where rim cements meet. Thin section. Sample 308-4-1, 126 cm.
Figure 4	Palisade rim cement followed by pore filling bladed crystals which show the typical blocky fabric of sparry calcite. Sample 308-4, CC.
Figures 5, 6	Fibrous low-Mg calcite rim cement in biogenous volcanic sandstone. In side view and under higher magnification the slender shape of the crystals is seen which taper only slightly towards the end because of very steep rhombohedral faces (Figure 6). SEM photomicrographs. Sample 308-4-1, 126 cm.

PLATE 2

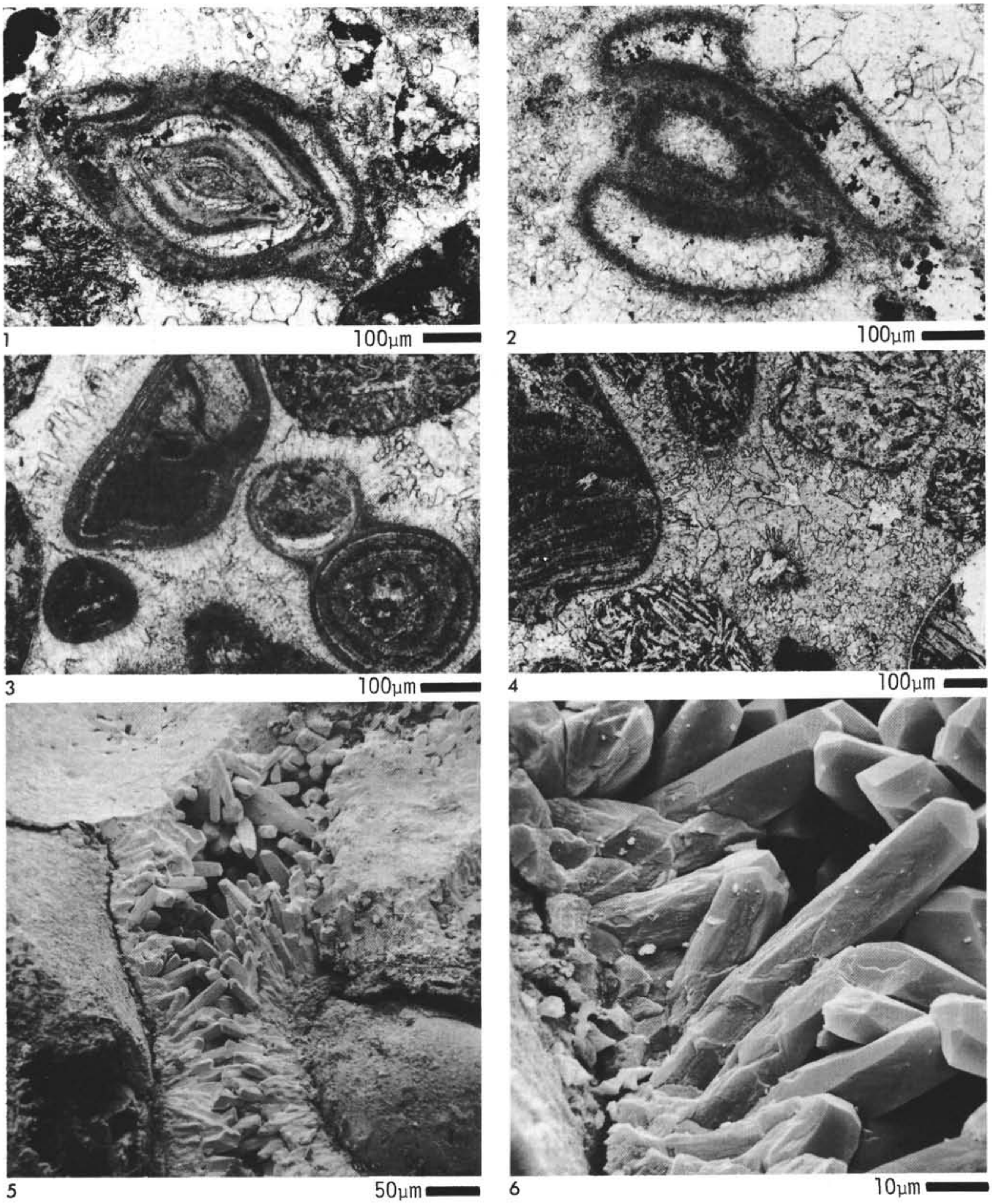

PLATE 3
Scanning electron photomicrographs of low-Mg crystals cementing biogenous volcanic sandstone.

Figure 1	Fibrous calcite with steep rhombohedral as well as curved faces on sides of crystals. The crystals often terminate with two sets of rhombohedral faces rotated against each other by 60°. Some of the crystals are composite ones. Sample 308-4-1, 126 cm.
Figure 2	Short fibrous crystals rooted on foraminiferal wall are overgrown by large-bladed composite crystals. Sample 308-4-1, 126 cm.
Figure 3	Surfaces of volcanic grains coated with box-work authigenic montmorillonite. Only few fibrous crystals grow on the montmorillonite substrate and large pore-filling second-generation bladed composite calcite may therefore be in indirect contact with detrital grain. No centripetal increase of crystal size is observed (Bathurst's rule not fulfilled). Sample 308-4, CC.
Figures 4-6	Subparallel radiating fibrous rim cement overgrown by bladed composite crystals. Figures 4 to 6 show progressive infilling of pore by second-generation bladed calcite. Notice step-like thinning of these crystals in Figure 5. Progressive growth of bladed crystals results in bulky texture (Figure 5) where single crystals are still recognizable and to a sparry mosaic where bladed crystal habit is no more recognizable. Sample 308-4, CC.

PLATE 3